The Atlantic Meridional Overturning Circulation and the Cabbeling Effect

FABIAN SCHLOESSER

University of Hawai'i at Mānoa, Honolulu, Hawaii

(Manuscript received 22 April 2020, in final form 1 July 2020)

ABSTRACT

North Atlantic meridional density gradients have been identified as a main driver of the Atlantic meridional overturning circulation (AMOC). Due to the cabbeling effect, these density gradients are increasingly dominated by temperature gradients in a warming ocean, and a direct link exists between North Atlantic mean temperature and AMOC strength. This paper quantifies the impact of this mechanism in the Stommel and Gnanadesikan models. Owing to different feedback mechanisms being included, a 1°C warming of North Atlantic mean ocean temperature strengthens the AMOC by 3% in the Gnanadesikan model and 8% in the Stommel model. In the Gnanadesikan model that increase is equivalent to a 4% strengthening of Southern Hemisphere winds and can compensate for a 14% increase in the hydrological cycle. Furthermore, mean temperature strongly controls a freshwater forcing threshold for the strong AMOC state, suggesting that the cabbeling effect needs to be considered to explain past and future AMOC variability.

1. Introduction

The Atlantic meridional overturning circulation (AMOC) is a key component of the Earth climate system. Dynamical considerations and model studies indicate that the AMOC strength is closely related to the meridional density gradient and thermocline depth in the North Atlantic (Johnson et al. 2019). Through meridional advection of heat and freshwater, the AMOC does not only affect climate patterns, but also influences ocean density and stratification, providing the opportunity for positive feedback mechanisms and nonlinear modes of climate variability (Stommel 1961; Broecker 1987; Stocker et al. 2001; Weijer et al. 2019).

Indeed, paleoclimate records indicate that the last glacial period was characterized by strong, irregular millennial variability associated with reorganizations of the AMOC, known as Dansgaard–Oeschger (DO) events (Dansgaard et al. 1993; Bond et al. 1999; Alley 2000; Andersen et al. 2004). No such variability occurs during warm periods, suggesting not only a link between mean states of climate and AMOC but also their stability.

In ocean and climate models, the AMOC is strongly impacted by freshwater fluxes into the ocean (Stommel 1961; Weaver et al. 1993; Stocker et al. 2001; Timmermann et al. 2003; Wolfe and Cessi 2014; Menviel et al. 2014). The AMOC can be turned off in such models by inducing a sufficiently large freshwater flux into the North Atlantic, mimicking the rapid retreat of Northern Hemisphere ice sheets. On the other hand, evidence from paleoclimate proxies on the timing of AMOC changes and iceberg transport suggests that meltwater did not always act as a trigger for AMOC events (Barker et al. 2015; Ng et al. 2018).

A number of other mechanisms have been proposed to explain the AMOC variability. The expansion of North Atlantic sea ice has been shown to impact the AMOC through its control over surface fluxes, and by affecting the locations where deep convection occurs (Stocker et al. 2001; Bitz et al. 2007; Sévellec and Fedorov 2015). The link between wind forcing and the AMOC has been explored, in particular in the North Atlantic and the Southern Ocean. It has also been shown that changes in basin geometry, like the opening and closing of the Bering Strait (Shaffer and Bendtsen 1994; Hu et al. 2012), can affect the AMOC behavior.

Denotes content that is immediately available upon publication as open access.

Supplemental information related to this paper is available at the Journals Online website: https://doi.org/10.1175/JPO-D-20-0085.s1.

Corresponding author: Fabian Schloesser, schloess@hawaii.edu

DOI: 10.1175/JPO-D-20-0085.1

The nonlinear equation of state for seawater has been noted to contribute to systematic AMOC changes under warming climate conditions in coupled climate models (Stouffer and Manabe 2003). De Boer et al. (2007) explore this mechanism in an idealized model, finding that while the AMOC is reduced, an increasingly strong Pacific meridional overturning circulation develops with increasing mean temperature. It is difficult, however, to isolate the effect of specific processes in complex climate models which often show substantial biases, and where many of the processes impacting the AMOC act concurrently.

Theoretical models have been developed to better understand and quantify the impact of different processes and forcings on the AMOC strength and stability. Despite their often simplistic design, such models have been remarkably successful in simulating the behavior of more sophisticated general circulation models (Weijer et al. 2019). The salt–advection feedback in the Stommel model (Stommel 1961) helps maintain a strong AMOC throughout the current climate, by reducing the meridional salinity difference. This feedback also allows, however, for a second stable state of the circulation without deep water formation in the North Atlantic. Furthermore, a strong, northward AMOC cannot be maintained if freshwater fluxes in the North Atlantic exceed a certain threshold.

A number of studies have expanded on the Stommel model, by including additional processes. Models with an additional Southern Hemisphere box (Rooth 1982; Rahmstorf 1996; Scott et al. 1999) highlight the importance of salt fluxes and freshwater fluxes for the interhemispheric overturning strength and stability. In a similar analytic framework, the Gnanadesikan model (Gnanadesikan 1999) includes dynamical constraints related to wind-driven upwelling and eddy fluxes in the Southern Ocean (Wyrtki 1961; Toggweiler and Samuels 1995), which provide a strong control over the AMOC strength (Cessi 2019; Johnson et al. 2019). A combination of Stommel and Gnanadesikan model constraints has been explored by Johnson et al. (2007) and Gnanadesikan et al. (2018).

A typical characteristic of these theoretical models is that temperature and salinity are competing for control over density gradients, and hence the strength and direction of the circulation. For example, the tropical reservoir is warm and salty compared to the subpolar reservoir in the Stommel model, and the Northern Hemisphere box is warm and salty compared to the Southern Hemisphere box in the Rooth model (Rooth 1982; Rahmstorf 1996; Scott et al. 1999). Consequently, the thermal expansion and haline contraction coefficients ought to be critical in determining model thresholds and behavior. However, a linear equation of state with constant values for both parameters is used in most analytic models. A study using a quadratic equation of state (Roquet et al. 2017) notes that it contributes to the instability properties of a loop model.

In general circulation models, nonlinearities in the equation of state (IOC et al. 2010) are critical to explain the present day stratification (Roquet et al. 2015; Nycander et al. 2015), most notably the thermobaric and cabbeling effects. The former describes the increase of thermal expansion of seawater with pressure, and the latter the increase with temperature. This study aims to quantify the impact of the cabbeling effect in the Stommel and Gnanadesikan models. In particular, it addresses the question whether there could exist a direct link between mean climate and overturning circulation through systematic changes in thermal expansion.

The remainder of the manuscript is organized as follows. Section 2 introduces the equation of state used in this study, and sections 3 and 4 explore the consequences of implementing this equation of state in the Stommel and Gnanadesikan models, respectively. Results are discussion in section 5.

2. Equation of state

A quadratic approximation to the density equation is used,

$$\rho = \rho_o - \alpha_o T - \frac{\alpha_1}{2T_o} T^2 + \beta S, \tag{1}$$

with $\alpha_o = 0.065\,\mathrm{kg\,m^{-3}\,K^{-1}}$, $\alpha_1 = 0.1\,\mathrm{kg\,m^{-3}\,K^{-1}}$, $T_o = 10°\mathrm{C}$, $\beta = 0.78\,\mathrm{kg\,m^{-3}\,PSU^{-1}}$, and $\rho_o = 1027.97\,\mathrm{kg\,m^{-3}}$ (Fig. 1), which provides a reasonable fit with the full equation of state (IOC et al. 2010). In this approximation, the thermal expansion coefficient $\alpha \equiv -d\rho/dT = \alpha_o + \alpha_1 T/T_o$ increases linearly with temperature. The density difference between a tropical and a subpolar reservoir is of particular interest in the present study, with the properties of the two reservoirs being indicated by subscripts "trop" and "subp," respectively. According to (1) this density difference can be written analog to a linear equation of state,

$$\Delta\rho = \overline{\alpha}\Delta T - \beta\Delta S, \qquad \overline{\alpha} \equiv \alpha_o + \alpha_1 \frac{\overline{T}}{T_o}, \tag{2}$$

with $\Delta\rho \equiv \rho_{\mathrm{subp}} - \rho_{\mathrm{trop}}$, $\Delta T \equiv T_{\mathrm{trop}} - T_{\mathrm{subp}}$, $\Delta S = S_{\mathrm{trop}} - S_{\mathrm{subp}}$, and $\overline{T} \equiv (T_{\mathrm{trop}} + T_{\mathrm{subp}})/2$. A useful property of the finite difference thermal expansion coefficient $\overline{\alpha}(\overline{T})$ is that it is independent of the temperature difference ΔT and equal to the thermal expansion coefficient at the mean temperature $\overline{T}$, i.e., $\overline{\alpha}(\overline{T}) = \alpha(\overline{T})$ (see Fig. 1a for an illustration of that property).

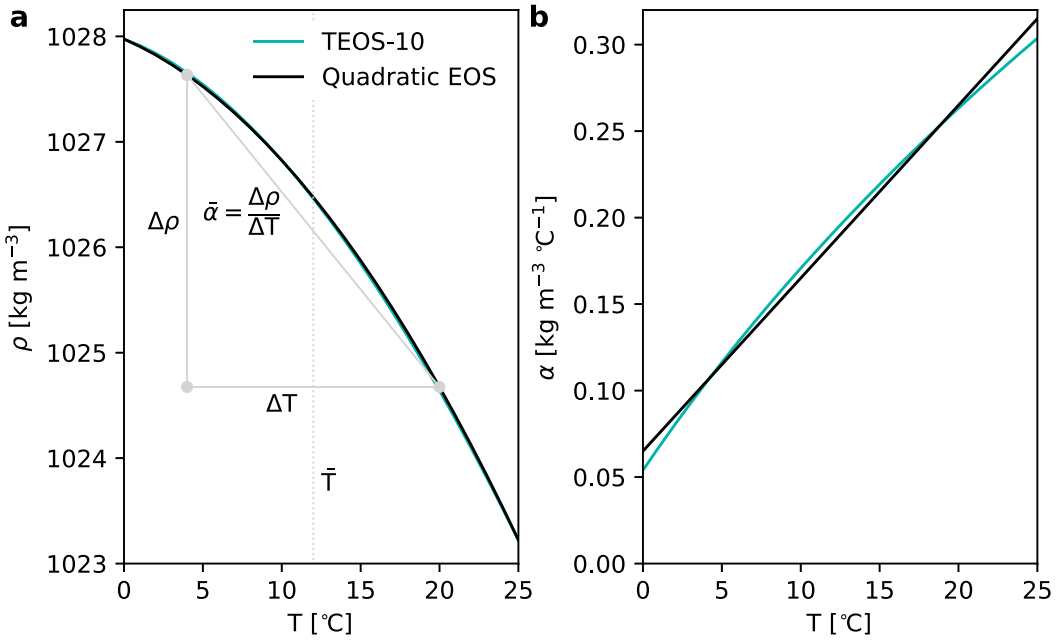

FIG. 1. Quadratic approximation to the equation of state: (a) density and (b) thermal expansion coefficient as a function of temperature with a constant salinity of 35 PSU at surface pressure calculated using the full equation of state (TEOS-10; IOC et al. 2010) and the quadratic approximation (1).

3. Stommel model

a. Model equations

The Stommel box model (Stommel 1961) consists of two well mixed reservoirs (Fig. 2), which exchange water at a rate

$$Q_N = k\Delta\rho = k(\bar{\alpha}\Delta T - \beta\Delta S), \tag{3}$$

proportional to the density difference between the two reservoirs calculated using (2), with $k = 10\,\mathrm{Sv\,m^3\,kg^{-1}}$ (all standard model parameter values are also given in Table 1). Only steady states are considered in this study. Accordingly, temperature and salinity are determined by a balance of surface forcing and advection. In the former case, the downward surface heat flux relaxes reservoir temperatures toward externally prescribed temperatures T^f_{trop} and T^f_{subp}. Specifically $|Q_N|\Delta T = -\gamma_{\mathrm{subp}}(T^f_{\mathrm{subp}} - T_{\mathrm{subp}})$ for the cold, subpolar reservoir and $|Q_N|\Delta T = \gamma_{\mathrm{trop}}(T^f_{\mathrm{trop}} - T_{\mathrm{trop}})$ for the warm, tropical reservoir, with the constants γ_{trop} and γ_{subp} reflecting reservoir sizes and strengths of the surface coupling. It is useful to write these temperature constraints in terms of temperature average and difference as they appear in (2),

$$\Delta T = \frac{\gamma}{2|Q_N| + \gamma}\Delta T^f, \quad \gamma \equiv \frac{2\gamma_{\mathrm{subp}}\gamma_{\mathrm{trop}}}{\gamma_{\mathrm{subp}} + \gamma_{\mathrm{trop}}}, \tag{4}$$

$$\overline{T} = \overline{T}^f + \frac{\mu|Q_N|}{2|Q_N| + \gamma}\Delta T^f, \quad \mu \equiv \frac{\gamma_{\mathrm{trop}} - \gamma_{\mathrm{subp}}}{\gamma_{\mathrm{trop}} + \gamma_{\mathrm{subp}}}, \tag{5}$$

with the external mean temperature $\overline{T}^f \equiv (T^f_{\mathrm{subp}} + T^f_{\mathrm{trop}})/2$ and external temperature difference $\Delta T^f \equiv T^f_{\mathrm{trop}} - T^f_{\mathrm{subp}} = 25°\mathrm{C}$. In the original Stommel model both reservoirs have the same size and $\gamma_{\mathrm{subp}} = \gamma_{\mathrm{trop}} = \gamma$. The constraint for the temperature difference (4) remains unchanged despite loosening this restriction, now using the effective relaxation parameter $\gamma = 80\,\mathrm{Sv}$ ($1\,\mathrm{Sv} = 10^6\,\mathrm{m^3\,s^{-1}}$). In the limit that one reservoir is much larger than the other and hence temperatures are much less affected by advection, e.g., $\gamma_{\mathrm{trop}} \gg \gamma_{\mathrm{subp}}$, one obtains $\gamma = 2\gamma_{\mathrm{subp}}$.

Constraint (5) is typically discarded, because Q_N is independent of $\overline{T}$ with a linear equation of state. For the original Stommel model ($\gamma_{\mathrm{subp}} = \gamma_{\mathrm{trop}}$) $\mu = 0$, and hence $\overline{T} = \overline{T}^f$ is externally prescribed, however, this is not the case in general. For the present day it appears that the case $\gamma_{\mathrm{trop}} > \gamma_{\mathrm{subp}}$ is most relevant: since the circulation is not closed in the South Atlantic and water upwells globally, it is already substantially warmed before entering the tropical Atlantic surface layer. In other words, water flowing northward is on average warmer than water flowing southward in the South Atlantic. This reduces tropical Atlantic temperature sensitivity to the AMOC strength compared to the hypothetical case that all water directly upwelled into the tropical Atlantic. Such complexity cannot be fully resolved in a two-box

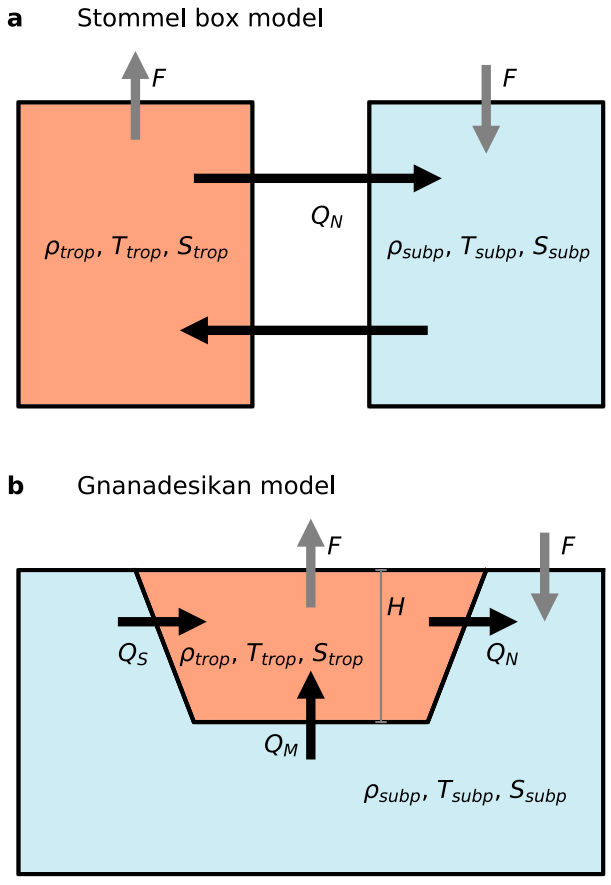

FIG. 2. Schematic illustration of the Stommel and Gnanadesikan models: (a) the Stommel box model (Stommel 1961) and (b) the Gnanadesikan model (Gnanadesikan 1999).

model, however, the effect can be approximated by setting $\mu > 0$ ($\mu \to 1$ in the limit that $\gamma_{\text{trop}} \to \infty$ and $T_{\text{trop}} \to T^f_{\text{trop}}$). Consistently, a strong Q_N is correlated with abnormally warm North Atlantic surface temperatures (Zhang et al. 2019).

For salinity driven circulations ($Q_N < 0$), the same parameters γ and μ may not be appropriate as with sinking in the subpolar box, because tropical Atlantic surface temperatures are directly impacted by the flow from the subpolar Atlantic (here the subpolar box may be less impacted, depending on the source water). In this study, steady-state solutions are obtained in terms of $\overline{T}$, hence no standard parameter values γ_{trop}, γ_{subp}, and μ are required, and solutions are valid independent of reservoir sizes. But one ought to be mindful about $\overline{T}$ being part of the solution. Furthermore, as an average North Atlantic temperature, it does not necessarily reflect the global mean. Constraint (5) can be used to calculate the corresponding externally imposed $\overline{T}^f$, or changes thereof, for any specific choice of reservoir size.

TABLE 1. Standard parameter values used in the model solutions [Stommel box model (S), Gnanadesikan model (G), or both], and their standard deviation in percentage of the standard value used for uncertainty estimates.

Parameter	Value	Model	STD
k	$10\,\text{Sv}\,\text{m}^3\,\text{kg}^{-1}$	S	—
γ	80 Sv	Both	100%
$\overline{T}$	12°C	Both	10%
ΔT^f	25°C	Both	20%
F	30 Sv PSU	Both	40%
k_N	$6 \times 10^{-5}\,\text{Sv}\,\text{m}\,\text{kg}^{-1}$	G	30%
Q_W	20 Sv	G	20%
k_E	$0.025\,\text{Sv}\,\text{m}^{-1}$	G	50%
k_M	4000 Sv m	G	50%

The salinity difference is maintained by a prescribed surface freshwater flux into the subpolar and out of the tropical reservoir (Fig. 2), balanced by advection,

$$F = |Q_N|\Delta S, \tag{6}$$

where $F = 30$ Sv PSU is the freshwater flux times the mean salinity. Effects of mean salinity changes are not considered here. For a given $\overline{T}$, constraints (3), (4) and (6) form a closed system of equations for the three variables Q_N, ΔT, and ΔS identical to the original Stommel model, despite the use of a nonlinear equation of state. The following analysis focuses on how changes in $\overline{T}$ and $\overline{\alpha}$ impact the solutions, in particular the stable one in which the density difference is dominated by temperature, $\overline{\alpha}\Delta T > \beta\Delta S$.

b. Solutions

Three solutions are shown in Fig. 3, corresponding to different levels of simplification from the full Stommel model, to illustrate the impact of processes. If advective temperature and salinity feedbacks are both neglected (red curves), i.e., Q_N is replaced by $Q_o = 20$ Sv in (4) and (6), ΔS and ΔT are both determined externally. Hence, the overturning strength Q_N increases linearly with $\overline{\alpha}$ and mean temperature $\overline{T}$.

Next, we include the impact of salinity advection feedback (blue curves in Fig. 3), by only replacing Q with Q_o in (4). Eliminating ΔS using (3) and (6) yields

$$Q_N = k\left(\overline{\alpha}\Delta T - \beta\frac{F}{|Q_N|}\right). \tag{7}$$

For $Q_N > 0$ solutions to the quadratic equation are

$$Q^+ = k\overline{\alpha}\Delta T\left[\frac{1}{2} \pm \sqrt{\frac{1}{4} - \frac{\beta F}{k(\overline{\alpha}\Delta T)^2}}\right]. \tag{8}$$

Only the first one of these two solutions is stable (Marotzke 2000), with $Q^+ \to k\overline{\alpha}\Delta T$ and $\Delta S \to 0$ in the

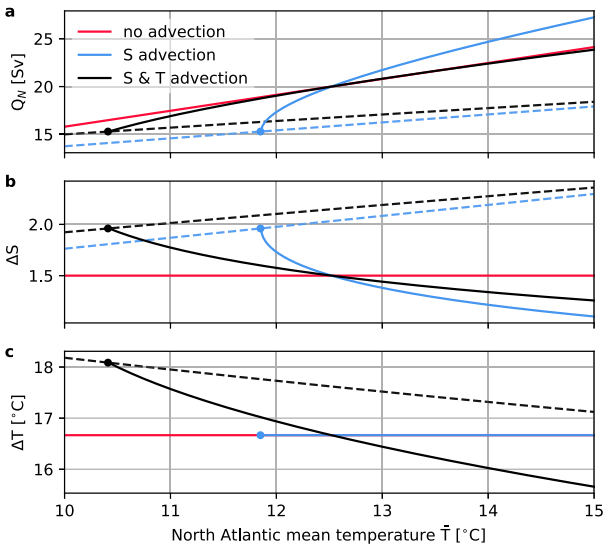

FIG. 3. Impact of mean temperature on the Stommel model: temperature dominated solutions ($Q_N > 0$) to the Stommel box model without advective feedbacks (red curves), with salt feedback (blue curves), and with salt and temperature advective feedbacks (black curves) as a function of mean temperature. (a) The strength of the overturning circulation, (b) the salinity difference, and (c) the temperature difference between the two boxes. Dashed curves indicate corresponding solutions with freshwater forcing set to its maximum threshold $F_m(\overline{T})$, and circles mark the thresholds T_m, where $F = F_m$.

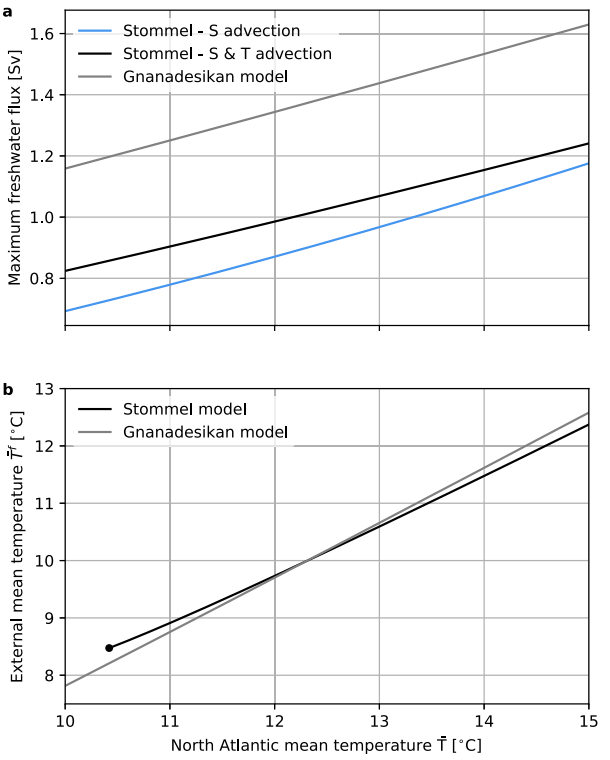

FIG. 4. Impact of mean temperature on the maximum freshwater forcing threshold: (a) maximum freshwater forcing threshold for solutions with $Q_N > 0$ as a function of mean temperature, i.e., F_m divided by a mean salinity of 35 PSU. Corresponding to Fig. 3, the blue curve indicates this threshold in the Stommel box model without and the black curve with temperature advection. The gray curve shows the same threshold for the Gnanadesikan model. (b) The external mean temperature $\overline{T}^f$ as a function of North Atlantic mean temperature $\overline{T}$ assuming $\mu = 0.75$. The circle marks the minimum temperatures for which the Stommel solution exists.

limit of $F \to 0$. Since ΔS is reduced with increasing Q_N, salt advection provides a positive feedback and amplifies the response to changes in mean temperature.

Temperature advection feedback has the opposite effect as that for salinity, because reduced temperature gradients weaken $\Delta\rho$, thereby reducing the sensitivity of Q^+ to $\overline{T}$ in the full Stommel box model (black curves; solutions obtained numerically). Reduced temperature differences with increased mean temperature (Fig. 3c) also imply that high latitudes warm faster than the tropics. For the parameters used, ΔT is reduced by about 0.5°C per 1°C of warming, i.e., higher latitudes warm almost twice as fast as the tropics. This illustrates, that while polar amplification of temperature acts as a negative feedback on AMOC strength, the AMOC strengthening in response to mean warming could contribute to polar amplification provided the circulation remains near equilibrium.

It follows directly from (8), that the radicand is positive and the strong AMOC state exists only for F below a maximum freshwater forcing threshold, that is for $F < F_m$ with

$$F_m = \frac{k(\overline{\alpha}\Delta T)^2}{4\beta}. \tag{9}$$

Without temperature advection feedback, the threshold F_m increases quadratically with $\overline{\alpha}$, and hence is strongly dependent on mean temperature (Fig. 4). When the temperature advection feedback is included, F_m increases similarly with $\overline{\alpha}$: taking the limit $F \to F_m$ and eliminating ΔT using (4) gives $Q^+ \to k\overline{\alpha}\Delta T/2 = \gamma/4(\sqrt{1 + 4k\overline{\alpha}\Delta T^f/\gamma} - 1)$, meaning Q^+ reaches a minimum in the limit $F \to F_m$. Consequently, the temperature advection feedback is relatively weak, and ΔT changes relatively slowly. Solutions with $F = F_m(\overline{T})$ are indicated by dashed curves in Fig. 3. The intersections of dashed and solid lines mark the temperature where $F_m(\overline{T})$ is equal to the standard value used. Hence, the standard solution exists only for mean temperatures higher than a threshold, $T_m(F)$, which is obtained by inverting (9) to mean temperature.

The mean temperature advection feedback (5) amplifies externally imposed mean temperature changes. Figure 4b illustrates a specific example with $\mu = 0.75$, which corresponds to the heat flux in the tropical box being 7 times as strong as that in the subpolar one.

For this choice, $\overline{T}$ increases about 16% faster than the external mean temperature $\overline{T}^f$. This positive feedback between Q_N and $\overline{T}$ has the effect to generally amplify AMOC and North Atlantic temperature variability. At least in the present model formulation, however, where $\overline{T}$ solely increases because T_{subp} warms faster than T_{trop} cools in response to an AMOC strengthening, temperature advection is still a net negative feedback. A linear stability analysis (Ruddick and Zhang 1996) was performed to confirm that all steady-state solutions discussed for the Stommel model with (2) are stable and no oscillatory climate modes exist (appendix A).

For completeness, the solution to (7) with a salinity dominated density gradient and upwelling in the subpolar box ($Q_N < 0$) is noted,

$$Q^- = k\overline{\alpha}\Delta T\left[\frac{1}{2} - \sqrt{\frac{1}{4} + \frac{\beta F}{k(\overline{\alpha}\Delta T)^2}}\right]. \tag{10}$$

Here, the solution with a + is discarded because it does not satisfy $Q_N < 0$. The absolute strength of Q^- is reduced with increasing $\overline{\alpha}$, i.e., Q^- increases (Fig. S1 in the online supplemental material), because the temperature term is growing relative to the salinity term in (3). Note that the curves for $Q^+(\overline{T})$ and $Q^-(\overline{T})$ from Fig. 3 and Fig. S1 can only be interpreted together as a bifurcation diagram for $\mu = 0$, e.g., the original Stommel model, such that $\overline{T} = \overline{T}^f$. Otherwise $\overline{T}$ for the same $\overline{T}^f$ is larger for Q^+, because of the circulation being generally stronger.

4. Gnanadesikan model

a. Model equations

While Q_N in the Stommel model is generally interpreted as a proxy for the AMOC, it lacks (among other things) processes related to the thermocline depth and adjustments, which have been found to be critical to simulate the ocean response to changes in boundary conditions (e.g., De Boer et al. 2010; Johnson et al. 2019). The Gnanadesikan model (Gnanadesikan 1999) summarizes the current understanding of the AMOC (Cessi 2019; Johnson et al. 2019) by considering thermocline depth and including dynamical constraints related to Southern Ocean westerly winds and diapycnal mixing (Robinson and Stommel 1959; Munk and Wunsch 1998).

Similar to the Stommel model, it has two reservoirs which are thought to be separated by an isopycnal surface (Fig. 2). Mass is exchanged between the reservoirs in the North Atlantic (transport Q_N) and the Southern Ocean (Q_S) where the isopycnal outcrops, and across the isopycnal surface via diapycnal mixing processes in the ocean interior (Q_M). These three transports depend on the thermocline depth H and density difference $\Delta\rho$ as follows,

$$Q_N = k_N\Delta\rho H^2, \tag{11}$$

$$Q_S = Q_W - Q_E = Q_W - k_E H, \tag{12}$$

$$Q_M = \frac{k_M}{H}, \tag{13}$$

with $k_N = 6 \times 10^{-5}\,\mathrm{Sv\,kg^{-1}\,m}$, Southern Ocean wind-driven transport $Q_W = 20\,\mathrm{Sv}$, $k_E = 0.025\,\mathrm{Sv\,m^{-1}}$, and $k_M = 4000\,\mathrm{Sv\,m}$. Note that different parameterizations have been proposed for all transports (e.g., Johnson et al. 2007; McCreary et al. 2016), and estimates for their exact contributions even for the present state of the circulation remain somewhat uncertain (Cessi 2019). An estimate of the impact of such uncertainties on the present results (appendix B) suggests, that they are qualitatively robust at least with respect to parameter values. The standard values above correspond to an eddy diffusivity of about $1000\,\mathrm{m^2\,s^{-1}}$ in the eddy transport Q_E, and a diapycnal diffusivity of about $1.5 \times 10^{-5}\,\mathrm{m^2\,s^{-1}}$.

The original Gnanadesikan model does not include explicit equations for temperature, salinity, and $\Delta\rho$, with the latter to be diagnosed from data or models. Here, $\Delta\rho$, ΔT, and ΔS are determined through (2), (4), and (6) as in the Stommel model. A similar combination of Stommel and Gnanadesikan models is used in Johnson et al. (2007) and Gnanadesikan et al. (2018). Further utilizing the constraint that mass is conserved in each reservoir in steady state,

$$Q_N = Q_S + Q_M, \tag{14}$$

solutions can be obtained numerically. In a general sense, this model can be understood as a Stommel model with an overturning strength depending on $\Delta\rho$ in a nonlinear way. Ruddick and Zhang (1996) show that such models have solutions equivalent to those of the original Stommel model and behave similarly, if the overturning function is monotonic and not "too wiggly." The present results support this interpretation.

b. Solutions

First, solutions are obtained that neglect advective feedbacks by setting the overturning strength to $Q_o = 20\,\mathrm{Sv}$ in the salinity and temperature equations, thereby prescribing ΔT and ΔS externally (red curves in Fig. 5). Accordingly, $\Delta\rho$ increases linearly with $\overline{\alpha}$ and $\overline{T}$. The overturning rate Q_N grows slower than $\Delta\rho$, however,

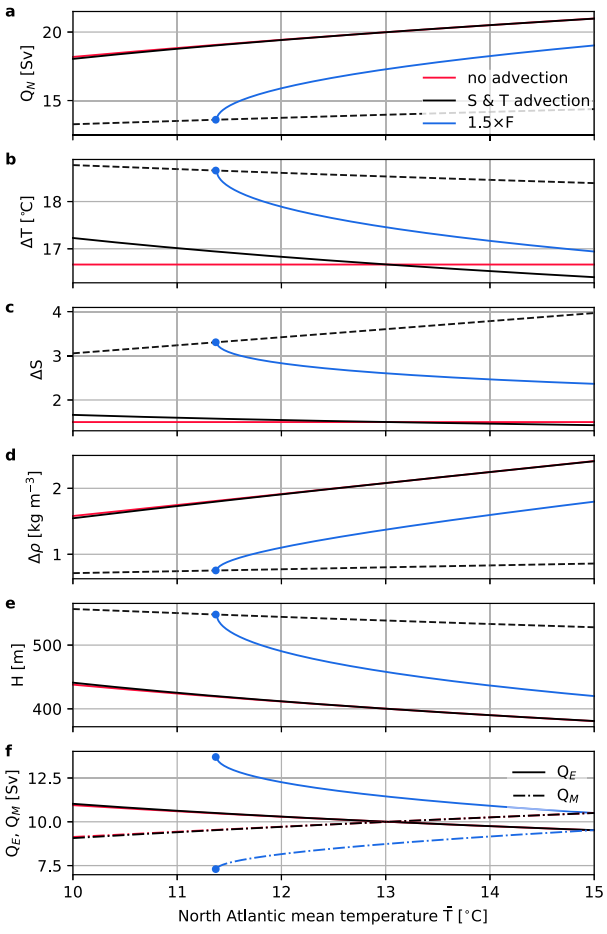

FIG. 5. Impact of mean temperature on the Gnanadesikan model: Temperature dominated solutions ($Q_N > 0$) to the Gnanadesikan model without (red curves) and with (black curves) advective temperature and salinity feedbacks. Blue curves indicate solutions with the freshwater forcing F increased by 50% for the full model, and dashed curves show solutions with the freshwater flux equal to its maximum threshold $F_m(\overline{T})$. Circles mark the threshold T_m, where $F = F_m$. (a) The strength of the overturning circulation, (b)–(d) the temperature, salinity, and density difference between the two boxes, and (e) the thermocline depth. (f) The transports driven by Southern Hemisphere eddies (Q_E, solid curves) and diapycnal mixing (Q_M, dash–dotted curves).

because the thermocline adjustment provides a negative feedback. This follows directly from the model equations, as substituting (12) and (13) in (14) yields Q_N as a monotonously decreasing function of the thermocline depth H. Increases in Q_N are compensated by decreased eddy transports Q_E and increased diapycnal mixing Q_M. A more complex response could occur, if Q_E and Q_M also were dependent on $\Delta\rho$.

When advective feedbacks are considered, and hence ΔT and ΔS determined internally, more than one solution exists as for the Stommel model. Again, the focus is on the solution with a temperature dominated $\Delta\rho$ and positive Q_N (black curves in Fig. 5). The effects of advective feedbacks for temperature and salinity on Q_N largely cancel each other for standard parameters, and Q_N increases by about 0.6 SV (3%) per 1°C of warming. Because of the reduced sensitivity of Q_N relative to the Stommel model, the polar amplification of warming is also weaker, with the subpolar reservoir warming by about 17% faster than the tropical reservoir. Likewise, the difference in changes between the external North Atlantic mean temperature and $\overline{T}$ is generally reduced (to 5% for parameters chosen in Fig. 4b).

The maximum freshwater forcing threshold F_m for solutions with $Q_N > 0$ is calculated numerically for the Gnanadesikan model (Fig. 4) and increases with $\overline{T}$ in a similar way as for the Stommel model. Because of the thermocline feedback, however, the threshold is generally higher and the forcing remains below this threshold for standard values. Solutions with freshwater forcing increased by 50% are shown (blue curves in Fig. 5) to illustrate that circulation and stratification are increasingly sensitive to changes in mean temperature as the threshold is approached.

To assess how effectively changes in mean ocean temperature impact the AMOC strength relative to changes in other boundary conditions, the following three measures are defined. First, M^Q is defined as the increase in overturning strength in percent caused by 1°C of warming of $\overline{T}$ (3% for standard parameters with $\overline{T} = 12$°C). Second, M^W is the increase in Southern Hemisphere wind forcing Q_W to accomplish the same increase in overturning strength as for 1°C of warming (4%). Finally, M^F is the increase in freshwater forcing required such that the overturning circulation remains constant under 1°C of warming (14%).

To test the sensitive of these results to the standard parameters used, M^Q, M^W, and M^F are recalculated using randomly sampled parameter values, constrained by the overturning strength being $15 \leq Q_N \leq 25$ Sv (appendix B). With a sample size of one million, the median and first and third quartiles for the results are $M^Q = 2.6\%$ (2.1%, 3.3%), $M^W = 4.0\%$ (3.1%, 5.3%), and $M^F = 16.0\%$ (12.1%, 21.7%), suggesting that the solutions obtained for standard values are qualitatively robust. Figure 6 illustrates the sensitivity to each parameter. The sensitivity to the mixing parameters k_M and k_E is relatively strong because of their control over the strength of the thermocline response to changes in Q_N in (14). Since k_M and k_E are integrals over the area of the ocean and the zonal extend of the Southern Ocean, respectively, this implies that sensitivities may be distorted in idealized general circulation model experiments with reduced basin size. For a more general discussion of the mixing parameters see also Johnson et al. (2007).

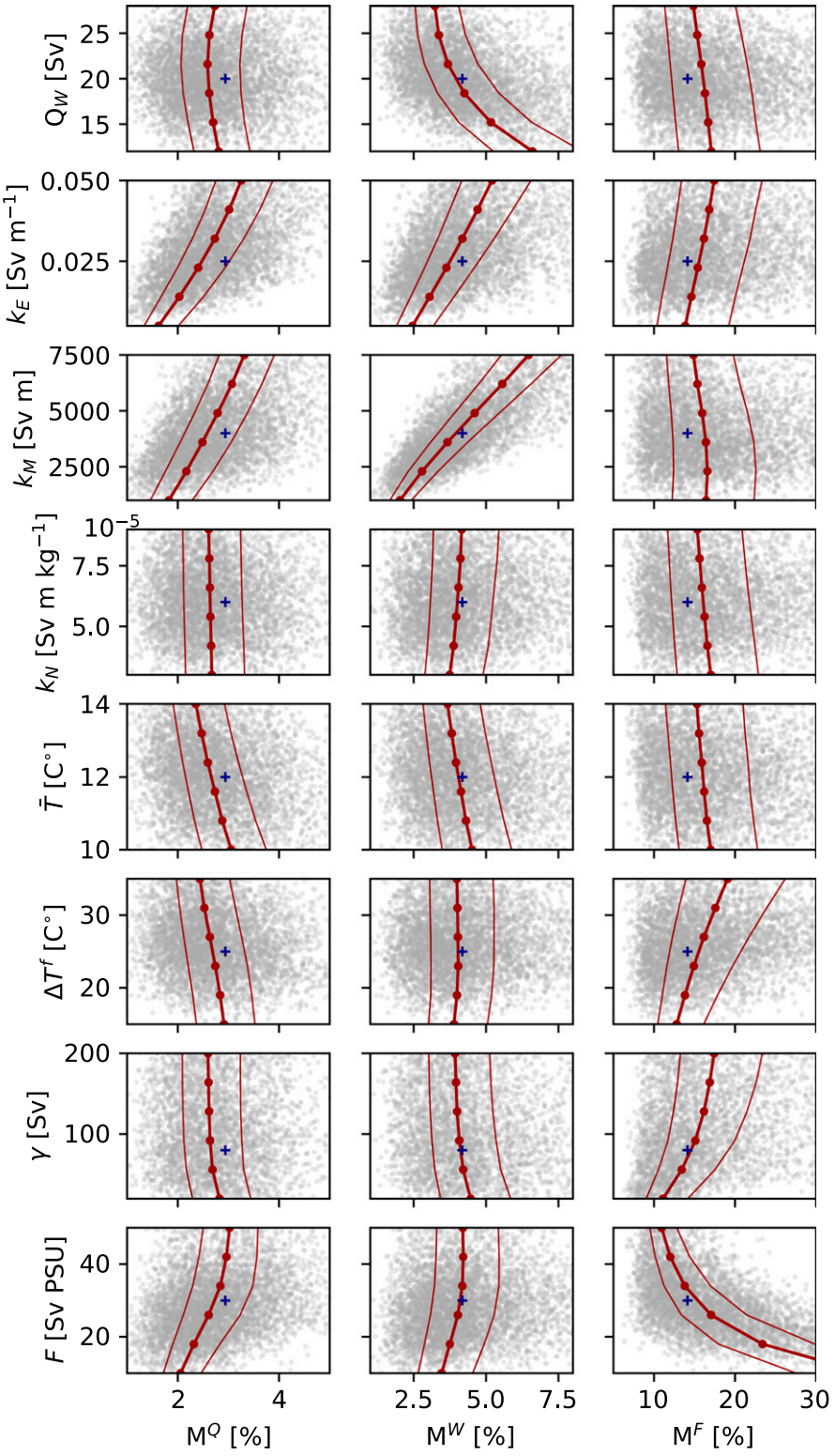

FIG. 6. Sensitivity of Gnanadesikan model results to model parameters: red curves show the median and first and third quartiles of the full set of solutions (N = 1 000 000) with randomly sampled parameter values (appendix B) as a function of each parameter. Gray dots show a subset of 5000 samples of the solutions, and blue plus signs indicate the standard parameter solution. Variables shown are M^Q, the increase in Q_N per 1°C increase in $\overline{T}$, M^W, the increase in Q_W required to increase Q_N by M^Q, and M^F, the increase in F required to keep Q_N constant with 1°C warming. Standard parameter values and corresponding standard deviations are given in Table 1.

Relative to that on AMOC strength, the impact on the freshwater threshold F_m is notably stronger for $\overline{T}$ than for Southern Hemisphere winds: while raising $\overline{T}$ by 1°C increases F_m by 7%, strengthening the winds by 4% increases F_m by only 2.3% for standard parameters. This is consistent with the equation for F_m in the Stommel model (9), which depends quadratically on the thermal expansion coefficient but only linearly on the parameter k, which describes the dynamical relation between the density difference and overturning strength (In contrast, the overturning strength, Eq. (3), depends linearly on both parameters). In the Gnanadesikan model the corresponding dynamical relation is substantially more complex because it involves the thermocline feedback and hence is for example affected by Southern Hemisphere winds. The relative sensitivities of F_m, however, appear to be largely preserved (Fig. S2 shows a near linear increase of F_m with Southern Hemisphere wind forcing, Q_W).

For completeness, the existence of a salinity driven AMOC state ($Q_N < 0$) is noted for the Gnanadesikan model (Fig. S3). Since all other transports must then be balanced by Q_E, a substantial deepening of the thermocline is required to reach that state. By substituting $Q_N < 0$ into (14) it follows that $H > 965$ m for the standard values. This state is very sensitive to the mean eddy diffusion in the Southern Ocean, a parameter that is not well constrained, in particular for circulation states that may substantially differ from present day.

c. Coupling to the deep overturning cell

So far, this study has neglected the interaction of the AMOC with the deep overturning cell. To fully consider that interaction requires at least one additional box to be included in the model, which is beyond the scope of the present manuscript. One main idea of how the deep cell impacts the AMOC is, however, by filling up the ocean basins with dense Antarctic Bottom Water, thereby squeezing the AMOC cell in the vertical (e.g., Shin et al. 2003; Jansen 2017; Sun et al. 2020). Here, the potential impact of this mechanism on the AMOC strength and stability are estimated, without addressing the processes that ultimately control the depth of the AMOC cell, and by ignoring potential impacts on the Southern Ocean closure (e.g., Wolfe and Cessi 2014).

(Schloesser et al. 2012) present a theory and idealized ocean general circulation model experiments, in which the depth of the AMOC cell H_D constrains its strength by introducing an additional factor into k_N, that is

$$Q_N = k_N \Delta\rho H^2, \quad k_N = k'_N \frac{H_D - H_m}{H_D}. \tag{15}$$

The underlying dynamical argument is that the thermocline is deepened by wave processes in the North Atlantic in response to the meridional density gradient, with mixing and instability processes acting against that deepening (Schloesser et al. 2012). Parameter H_m describes the increased North Atlantic thermocline depth and provides a measure for the strength of Rossby wave damping, which was empirically determined for idealized experiments. Unfortunately, H_m is not well constrained in general, implying the following estimate needs to be taken with a grain of salt. Assuming H_D is reduced from 3500 to 2000 m, roughly corresponding to the change from present day to the last glacial maximum (Lynch-Stieglitz et al. 2007), and allowing the thermocline to reach twice its tropical depth, $H_m = 2H$ (a choice consistent with the idealized ocean general circulation experiments reported in Schloesser et al. 2012), reduces k_N by 27%. This weakens the AMOC by 2.1 Sv (11%) in the solutions with standard parameters, equivalent to lowering $\overline{T}$ by 2.9°C.

Compared to that of the overturning strength, the sensitivity of threshold F_m to squeezing is weaker than to mean temperature. Somewhat similar to wind forcing, the squeezing affects the dynamical relation between overturning strength and density difference, k_N, and F_m depends linearly on k_N and quadratically on $\overline{\alpha}$ in (9). Specifically, the same changes in k_N and $\overline{T}$ as above result in 9% and 20% reductions in F_m in the Gnanadesikan model, respectively. Nonetheless, this example illustrates that, assuming (15) accurately describes the impact of the relation between AMOC depth and strength, interaction with the deep overturning cell can substantially contribute to AMOC strength and variability, in particular in concert with North Atlantic temperature changes.

5. Discussion

A link between the North Atlantic mean temperature and the AMOC has been observed in paleoclimate records as well as general circulation models (Sarnthein et al. 1994; Alley et al. 1999). The present results illustrate how increasing North Atlantic mean temperatures strengthen the large-scale meridional density gradient via the cabbeling effect, thereby increasing equilibrium AMOC strength. This mechanism could substantially contribute to modulating AMOC and North Atlantic temperature variability.

Paleoclimate records reveal that the occurrence of strong, millennial-scale variability, so-called Dansgaard–Oeschger (DO) events, is limited to cooler climates (Dansgaard et al. 1993; Bond et al. 1999; Alley 2000; Andersen et al. 2004). This variability, which involves a strong AMOC reduction or shut down, has been

associated with the existence of a maximum freshwater forcing threshold F_m in the Stommel model. General circulation model studies have confirmed the idea that the AMOC can be shut down by imposing sufficiently large freshwater fluxes (Weaver et al. 1993; Stocker et al. 2001; Timmermann et al. 2003; Wolfe and Cessi 2014; Menviel et al. 2014). Paleoclimate evidence, on the other hand, does not support the hypothesis that meltwater always acted as a trigger for DO events (Barker et al. 2015; Ng et al. 2018).

The present results suggest that the magnitude of the freshwater threshold F_m depends on a number of climate variables, and strongly so on North Atlantic mean temperature. Due to the cabbeling effect, F_m substantially increases with North Atlantic mean temperature (Fig. 4). A corollary is that the AMOC could then also be shut down by keeping freshwater forcing and other boundary conditions constant and applying a sufficiently strong cooling to the ocean. Since in reality one forcing or boundary condition will rarely change in isolation, a more general implication is that the cabbeling effect provides an explanation for, or contributes to, colder climate states being more susceptible to AMOC shutdown events.

Because of the AMOC feedback on North Atlantic ocean mean temperature, (5), the cabbeling effect tends to enhance AMOC and North Atlantic temperature variability slow enough for the AMOC–mean temperature feedback to be effective. Consider, for example, the response to strengthening Southern Hemisphere winds in an ocean general circulation model. Consistent with the Gnanadesikan model, the associated strengthening of the AMOC should lead to a warming of North Atlantic, which would cause a further strengthening of the AMOC. The observed sea surface temperature pattern related to AMOC strength (Zhang et al. 2019) is characterized by general warming in the North Atlantic that is enhanced in the subpolar region. This is consistent with the present model results (note, however, that in contrast to increasing mean temperatures, the polar amplification provides a negative feedback to the AMOC), suggesting that the cabbeling mechanism may be of relevance for variability on multidecadal time scales.

On the other hand, a substantial increase in temperature is projected for the twenty-first century together with a decrease in AMOC strength (Weijer et al. 2020). Likely explanations for this discrepancy include that ocean boundary conditions change too rapidly for the system to remain near equilibrium (Stouffer and Manabe 2003), and for the cabbeling mechanism to be overwhelmed by changes in other boundary conditions. In fact, some ocean general circulation models do show the AMOC equilibrium strength increasing with temperature (e.g., Jansen et al. 2018), although it is not clear how much of this can be attributed to the cabbeling effect.

The results presented in this study come with several caveats. The models used are extremely idealized, and lack spatial resolution and a number of processes that have been associated with AMOC strength and variability, for example sea ice, coupling with the deep overturning cell, or the Bering Strait. For this reason, quantitative results have to be treated with caution, and it cannot be deduced that the North Atlantic mean temperature exerts a dominant control over the AMOC strength via the cabbeling effect. Likely the real AMOC variability is caused by a combination of different processes acting in concert. The present results suggest, that the contribution of the cabbeling effect may not be negligible.

Acknowledgments. This research was supported by the NSF under Award 1903197. I thank Anand Gnanadesikan and one anonymous reviewer for their helpful comments.

Data availability statement. All data will be shared upon request.

APPENDIX A

Instability Analysis

A linear stability analysis for solutions to the Stommel box model with $Q_N > 0$ is preformed following Ruddick and Zhang (1996). Accordingly, the three Eigen values λ_i of the matrix $\mathbf{A}$ are calculated numerically, with the matrix elements being

$$\mathbf{A}_{ji} \equiv \frac{\partial X_j}{\partial x_i}, \tag{A1}$$

with

$$X_1 \equiv \frac{\partial \Delta T}{\partial t} = -\left(\frac{V_{\text{subp}} + V_{\text{trop}}}{V_{\text{subp}} V_{\text{trop}}} Q + \gamma'\right)\Delta T + \gamma' \Delta T^f, \tag{A2}$$

$$X_2 \equiv \frac{\partial \Delta S}{\partial t} = \frac{V_{\text{trop}} + V_{\text{subp}}}{V_{\text{trop}} V_{\text{subp}}}(F - Q\Delta S), \tag{A3}$$

$$X_3 \equiv \frac{\partial \overline{T}}{\partial t} = \frac{V_{\text{trop}} - V_{\text{subp}}}{2V_{\text{trop}} V_{\text{subp}}} Q\Delta T + \gamma' \overline{T}^f - \gamma' \overline{T}, \tag{A4}$$

and $(x_1, x_2, x_3) \equiv (\Delta T, \Delta S, \overline{T})$. Parameters V_{trop} and V_{subt} represent the volume of the tropical and subpolar reservoirs, and $\gamma' \equiv \gamma 2V_{\text{subp}}V_{\text{trop}}/(V_{\text{subp}} + V_{\text{trop}})$.

The analysis is performed assuming $V_{trop} \gg V_{subp}$ (specifically $V_{trop} = 10^6 V_{subp}$), thereby allowing for maximum positive feedback in (5). The eigenvalues for the solutions with standard parameter values are shown in Fig. S4 and scale linearly with the total volume $V_{subp} + V_{trop} = 10^{13}\,m^3$. The eigenvalues are all real and negative, meaning that solutions are stable and no oscillatory modes exist.

APPENDIX B

Uncertainty Estimate

To estimate the uncertainty associated with model parameter choices in the Gnanadesikan model M^Q (the increase in Q_N per 1°C increase of $\overline{T}$), M^W (the increase in Q_W required to increase Q_N by M^Q), and M^F (the increase in F required to keep Q_N constant with 1°C increase of $\overline{T}$) for a range of parameter values. Specifically, parameters are sampled from lognormal distributions with the median given by the standard value and standard deviation for each parameter given in Table 1. Only parameter sets yielding an overturning strength of $15 \leq Q_N \leq 25$ Sv are accepted. Note that while parameter values are sampled independently, parameter values for accepted parameter sets are no longer fully independent due to the overturning strength criterium. With an accepted sample size N of one million, the median and first and third quartiles for the results are $M^Q = 2.6\%$ (2.1%, 3.3%), $M^W = 4.0\%$ (3.1%, 5.3%), and $M^F = 16.0\%$ (12.1%, 21.7%). Results as a function of each parameter are shown in Fig. 6.

REFERENCES

Alley, R. B., 2000: Ice-core evidence of abrupt climate changes. *Proc. Natl. Acad. Sci. USA*, **97**, 1331–1334, https://doi.org/10.1073/PNAS.97.4.1331.

——, P. U. Clark, L. D. Keigwin, and R. S. Webb, 1999: Making sense of millennial-scale climate change. *Mechanisms of Global Climate Change at Millennial Time Scales, Geophys. Monogr.*, Vol. 112, Amer. Geophys. Union, 385–394.

Andersen, K., and Coauthors, 2004: High-resolution record of Northern Hemisphere climate extending into the last interglacial period. *Nature*, **431**, 147–151, https://doi.org/10.1038/nature02805.

Barker, S., J. Chen, X. Gong, L. Jonkers, G. Knorr, and D. Thornalley, 2015: Icebergs not the trigger for North Atlantic cold events. *Nature*, **520**, 333–336, https://doi.org/10.1038/NATURE14330.

Bitz, C., J. Chiang, W. Cheng, and J. Barsugli, 2007: Rates of thermohaline recovery from freshwater pulses in modern, Last Glacial Maximum, and greenhouse warming climates. *Geophys. Res. Lett.*, **34**, L07708, https://doi.org/10.1029/2006GL029237.

Bond, G. C., W. Showers, M. Elliot, M. Evans, R. Lotti, I. Hajdas, G. Bonani, and S. Johnson, 1999: The North Atlantic's 1-2 kyr climate rhythm: Relation to Heinrich Events, Dansgaard/Oeschger cycles and the little ice age. *Mechanisms of Global Climate Change at Millennial Time Scales, Geophys. Monogr.*, Vol. 112, Amer. Geophys. Union, 35–58.

Broecker, W. S., 1987: Unpleasant surprises in the greenhouse? *Nature*, **328**, 123–126, https://doi.org/10.1038/328123A0.

Cessi, P., 2019: The global overturning circulation. *Annu. Rev. Mar. Sci.*, **11**, 249–270, https://doi.org/10.1146/ANNUREV-MARINE-010318-095241.

Dansgaard, W., and Coauthors, 1993: Evidence for general instability of past climate from a 250-kyr ice-core record. *Nature*, **364**, 218–220, https://doi.org/10.1038/364218A0.

De Boer, A. M., D. M. Sigman, J. Toggweiler, and J. Russell, 2007: Effect of global ocean temperature change on deep ocean ventilation. *Paleoceanography*, **22**, PA2210, https://doi.org/10.1029/2005PA001242.

——, A. Gnanadesikan, N. R. Edwards, and A. J. Watson, 2010: Meridional density gradients do not control the Atlantic overturning circulation. *J. Phys. Oceanogr.*, **40**, 368–380, https://doi.org/10.1175/2009JPO4200.1.

Gnanadesikan, A., 1999: A simple predictive model for the structure of the oceanic pycnocline. *Science*, **283**, 2077–2079, https://doi.org/10.1126/SCIENCE.283.5410.2077.

——, R. Kelson, and M. Sten, 2018: Flux correction and overturning stability: Insights from a dynamical box model. *J. Climate*, **31**, 9335–9350, https://doi.org/10.1175/JCLI-D-18-0388.1.

Hu, A., and Coauthors, 2012: Role of the Bering Strait on the hysteresis of the ocean conveyor belt circulation and glacial climate stability. *Proc. Natl. Acad. Sci. USA*, **109**, 6417–6422, https://doi.org/10.1073/PNAS.1116014109.

IOC, SCOR, and IAPSO, 2010: The international thermodynamic equation of seawater – 2010: Calculation and use of thermodynamic properties. Intergovernmental Oceanographic Commission, Manuals and Guides 56, UNESCO, 196 pp., http://www.teos-10.org/pubs/TEOS-10_Manual.pdf.

Jansen, M. F., 2017: Glacial ocean circulation and stratification explained by reduced atmospheric temperature. *Proc. Natl. Acad. Sci. USA*, **114**, 45–50, https://doi.org/10.1073/PNAS.1610438113.

——, L.-P. Nadeau, and T. M. Merlis, 2018: Transient versus equilibrium response of the ocean's overturning circulation to warming. *J. Climate*, **31**, 5147–5163, https://doi.org/10.1175/JCLI-D-17-0797.1.

Johnson, H. L., D. P. Marshall, and D. A. Sproson, 2007: Reconciling theories of a mechanically driven meridional overturning circulation with thermohaline forcing and multiple equilibria. *Climate Dyn.*, **29**, 821–836, https://doi.org/10.1007/S00382-007-0262-9.

——, P. Cessi, D. P. Marshall, F. Schloesser, and M. A. Spall, 2019: Recent contributions of theory to our understanding of the Atlantic meridional overturning circulation. *J. Geophys. Res. Oceans*, **124**, 5376–5399, https://doi.org/10.1029/2019JC015330.

Lynch-Stieglitz, J., and Coauthors, 2007: Atlantic meridional overturning circulation during the Last Glacial Maximum. *Science*, **316**, 66–69, https://doi.org/10.1126/SCIENCE.1137127.

Marotzke, J., 2000: Abrupt climate change and thermohaline circulation: Mechanisms and predictability. *Proc. Natl. Acad. Sci. USA*, **97**, 1347–1350, https://doi.org/10.1073/PNAS.97.4.1347.

McCreary, J. P., R. Furue, F. Schloesser, T. W. Burkhardt, and M. Nonaka, 2016: Dynamics of the Atlantic meridional overturning circulation and Southern Ocean in an ocean model of intermediate complexity. *Prog. Oceanogr.*, **143**, 46–81, https://doi.org/10.1016/J.POCEAN.2016.01.001.

Menviel, L., A. Timmermann, T. Friedrich, and M. H. England, 2014: Hindcasting the continuum of Dansgaard–Oeschger variability: Mechanisms, patterns and timing. *Climate Past*, **10**, 63–77, https://doi.org/10.5194/CP-10-63-2014.

Munk, W., and C. Wunsch, 1998: Abyssal recipes II: Energetics of tidal and wind mixing. *Deep-Sea Res. I*, **45**, 1977–2010, https://doi.org/10.1016/S0967-0637(98)00070-3.

Ng, H. C., L. F. Robinson, J. F. McManus, K. J. Mohamed, A. W. Jacobel, R. F. Ivanovic, L. J. Gregoire, and T. Chen, 2018: Coherent deglacial changes in western Atlantic Ocean circulation. *Nat. Commun.*, **9**, 2947, https://doi.org/10.1038/S41467-018-05312-3.

Nycander, J., M. Hieronymus, and F. Roquet, 2015: The nonlinear equation of state of sea water and the global water mass distribution. *Geophys. Res. Lett.*, **42**, 7714–7721, https://doi.org/10.1002/2015GL065525.

Rahmstorf, S., 1996: On the freshwater forcing and transport of the Atlantic thermohaline circulation. *Climate Dyn.*, **12**, 799–811, https://doi.org/10.1007/S003820050144.

Robinson, A., and H. Stommel, 1959: The oceanic thermocline and the associated thermohaline circulation. *Tellus*, **11**, 295–308, https://doi.org/10.3402/tellusa.v11i3.9317.

Rooth, C., 1982: Hydrology and ocean circulation. *Prog. Oceanogr.*, **11**, 131–149, https://doi.org/10.1016/0079-6611(82)90006-4.

Roquet, F., G. Madec, L. Brodeau, and J. Nycander, 2015: Defining a simplified yet "realistic" equation of state for seawater. *J. Phys. Oceanogr.*, **45**, 2564–2579, https://doi.org/10.1175/JPO-D-15-0080.1.

——, R. Lindqvist, F. Pollmann, D. Ferreira, and G. Madec, 2017: Stability of the thermohaline circulation examined with a one-dimensional fluid loop. *Tellus*, **69A**, 1380490, https://doi.org/10.1080/16000870.2017.1380490.

Ruddick, B., and L. Zhang, 1996: Qualitative behavior and non-oscillation of Stommel's thermohaline box model. *J. Climate*, **9**, 2768–2777, https://doi.org/10.1175/1520-0442(1996)009<2768:QBANOS>2.0.CO;2.

Sarnthein, M., K. Winn, S. J. Jung, J.-C. Duplessy, L. Labeyrie, H. Erlenkeuser, and G. Ganssen, 1994: Changes in east Atlantic deepwater circulation over the last 30,000 years: Eight time slice reconstructions. *Paleoceanography*, **9**, 209–267, https://doi.org/10.1029/93PA03301.

Schloesser, F., R. Furue, J. P. McCreary, and A. Timmermann, 2012: Dynamics of the Atlantic meridional overturning circulation. Part I: Buoyancy-forced response. *Prog. Oceanogr.*, **101**, 33–62, https://doi.org/10.1016/J.POCEAN.2012.01.002.

Scott, J. R., J. Marotzke, and P. H. Stone, 1999: Interhemispheric thermohaline circulation in a coupled box model. *J. Phys. Oceanogr.*, **29**, 351–365, https://doi.org/10.1175/1520-0485(1999)029<0351:ITCIAC>2.0.CO;2.

Sévellec, F., and A. V. Fedorov, 2015: Unstable AMOC during glacial intervals and millennial variability: The role of mean sea ice extent. *Earth Planet. Sci. Lett.*, **429**, 60–68, https://doi.org/10.1016/J.EPSL.2015.07.022.

Shaffer, G., and J. Bendtsen, 1994: Role of the Bering Strait in controlling North Atlantic ocean circulation and climate. *Nature*, **367**, 354–357, https://doi.org/10.1038/367354A0.

Shin, S.-I., Z. Liu, B. L. Otto-Bliesner, J. E. Kutzbach, and S. J. Vavrus, 2003: Southern Ocean sea-ice control of the glacial North Atlantic thermohaline circulation. *Geophys. Res. Lett.*, **30**, 1096, https://doi.org/10.1029/2002GL015513.

Stocker, T. F., R. Knutti, and G.-K. Plattner, 2001: The future of the thermohaline circulation—A perspective. *The Oceans and Rapid Climate Change: Past, Present, and Future, Geophys. Monogr.*, Vol. 126, Amer. Geophys. Union, 277–293.

Stommel, H. M., 1961: Thermohaline convection with two stable regimes of flow. *Tellus*, **13**, 224–230, https://doi.org/10.3402/tellusa.v13i2.9491.

Stouffer, R., and S. Manabe, 2003: Equilibrium response of thermohaline circulation to large changes in atmospheric CO_2 concentration. *Climate Dyn.*, **20**, 759–773, https://doi.org/10.1007/S00382-002-0302-4.

Sun, S., I. Eisenman, L. Zanna, and A. L. Stewart, 2020: Surface constraints on the depth of the Atlantic meridional overturning circulation: Southern Ocean versus North Atlantic. *J. Climate*, **33**, 3125–3149, https://doi.org/10.1175/JCLI-D-19-0546.1.

Timmermann, A., M. Schulz, H. Gildor, and E. Tziperman, 2003: Coherent resonant millennial-scale climate transitions triggered by massive meltwater pulses. *J. Climate*, **16**, 2569–2585, https://doi.org/10.1175/1520-0442(2003)016<2569:CRMCOT>2.0.CO;2.

Toggweiler, J., and B. Samuels, 1995: Effect of Drake Passage on the global thermohaline circulation. *Deep-Sea Res. I*, **42**, 477–500, https://doi.org/10.1016/0967-0637(95)00012-U.

Weaver, A. J., J. Marotzke, P. F. Cummins, and E. S. Sarachik, 1993: Stability and variability of the thermohaline circulation. *J. Phys. Oceanogr.*, **23**, 39–60, https://doi.org/10.1175/1520-0485(1993)023<0039:SAVOTT>2.0.CO;2.

Weijer, W., and Coauthors, 2019: Stability of the Atlantic Meridional Overturning Circulation: A review and synthesis. *J. Geophys. Res. Oceans*, **124**, 5336–5375, https://doi.org/10.1029/2019JC015083.

——, W. Cheng, O. A. Garuba, A. Hu, and B. T. Nadiga, 2020: CMIP6 models predict significant 21st century decline of the Atlantic Meridional Overturning Circulation. *Geophys. Res. Lett.*, **47**, e2019GL086075, https://doi.org/10.1029/2019GL086075.

Wolfe, C. L., and P. Cessi, 2014: Salt feedback in the adiabatic overturning circulation. *J. Phys. Oceanogr.*, **44**, 1175–1194, https://doi.org/10.1175/JPO-D-13-0154.1.

Wyrtki, K., 1961: The thermohaline circulation in relation to general circulation in the oceans. *Deep-Sea Res.*, **8**, 39–64, https://doi.org/10.1016/0146-6313(61)90014-4.

Zhang, R., R. Sutton, G. Danabasoglu, Y.-O. Kwon, R. Marsh, S. G. Yeager, D. E. Amrhein, and C. M. Little, 2019: A review of the role of the Atlantic Meridional Overturning Circulation in Atlantic multidecadal variability and associated climate impacts. *Rev. Geophys.*, **57**, 316–375, https://doi.org/10.1029/2019RG000644.